ISSN 1027-5495. Functional Materials, 27, No.4 (2020), p. 736-743.
doi:https://doi.org/10.15407/fm27.04.736

Structural engineering of multi-period (TiMo)N/ZrN vacuum arc coatings

***O.V.Sobol*[1], *N.V.Pinchuk*[1], *A.A.Meylekhov*[1], *V.V.Subbotina*[1], *Osman Dur*[2], *V.A.Stolbovoy*[3], *D.V.Kovteba*[3]**

[1]National Technical University "Kharkiv Polytechnic Institute",
2 Kyrpychova St., 61002 Kharkiv,Ukraine
[2]Hacettepe University Technopolis, Universiteler Mahallesi 1596. Cadde 6.
F-Book Kat:3 Beytepe, 06800 Ankara, Turkey
[3]National Science Center Kharkiv Institute of Physics and Technology,
1 Akademicheskaya St., 61108 Kharkiv, Ukraine

Received April 28, 2020

The effect of the bias potential applied to the substrate during deposition and the layer thickness on the elemental composition, structure, substructure, and stress-strain state of (TiMo)N/ZrN layers of multi-period coatings is studied. The results of elemental analysis indicate a decrease in the ratio (Ti + Mo)/Zr with an increase in the bias potential and with a decrease in the layer thickness. At the structural level, appearance of additional diffraction peaks for (TiMo)N/ZrN coatings with the thinnest (about 12 nm) layers was revealed. The appearance of such peaks is explained by the effect of mixing at the interface between layers due to the implantation of accelerated particles. It was found that alloying of Ti with Mo atoms in (TiMo)N layers leads to a large compression strain (about 5 %). In monometallic ZrN layers, the value of macrostrain is more than 2 times smaller. At the substructural level, the formation of (TiMo)N solid solution also leads to higher microdeformation in comparison with a similar parameter in ZrN monometallic layers. The hardness of multi-period (TiMo)N/ZrN composites reaches a high value of 35 GPa.

Keywords: structural engineering, vacuum arc technology, coating, Layer thickness, bias potential, structure, substructure, stress-strain state, hardness.

Структурна інженерія багатоперіодних (TiMo)N/ZrN вакуумно-дугових покриттів. *О.В.Соболь, Н.В.Пінчук, А.О.Мейлехов, В.В.Субботіна, Osman Dur, В.О.Столбовий, Д.В.Ковтеба*

Досліджено вплив потенціалу зміщення, що подається на підкладку при осадженні, і товщини шарів на елементний склад, структуру, субструктуру і напружено-деформований стан шарів (TiMo)N/ZrN багатоперіодних покриттів. Результати елементного аналізу свідчать про зменшення відношення (Ti+Mo)/Zr зі збільшенням потенціалу зміщення і при зменшенні товщини шару. Подібний ефект збільшення відносного вмісту більш важких атомів також виявлено і для співвідношення Ti/Mo. На структурному рівні виявлено появу додаткових дифракційних піків для (TiMo)N/ZrN покриттів з найбільш тонкими (близько 12 нм) шарами. Появу таких піків пояснено ефектом перемішування на границі розділу шарів внаслідок імплантації прискорених частинок. Встановлено, що легування Ti атомами Mo в (TiMo)N шарах призводить до великої деформації стиснення (близько 5 %). У монометалевих ZrN шарах величина макродеформації більш, ніж у 2 рази менше. На субструктурному рівні формування (TiMo)N твердого розчину також призводить до більш високої мікродеформації у порівнянні з аналогічним параметром у ZrN монометалевих шарах. Твердість багатоперіодних (TiMo)N/ZrN композитів досягає великої величини 35 ГПа.

Исследовано влияние потенциала смещения, подаваемого на подложку при осаждении, и толщины слоев на элементный состав, структуру, субструктуру и напряженно-деформированное состояние слоев (TiMo)N/ZrN многопериодных покрытий. Результаты элементного анализа свидетельствуют об уменьшении отношения (Ti + Mo)/Zr с увеличением потенциала смещения и при уменьшении толщины слоя. Подобный эффект увеличения относительного содержания более тяжелых атомов также выявлен и для соотношения Ti/Mo. На структурном уровне выявлено появление дополнительных дифракционных пиков для (TiMo)N/ZrN покрытий с наиболее тонкими (около 12 нм) слоями. Появление таких пиков объяснено эффектом перемешивания на границе раздела слоев вследствие имплантации ускоренных частиц. Установлено, что легирование Ti атомами Mo в (TiMo)N слоях приводит к большой деформации сжатия (около 5 %). В монометаллических ZrN слоях величина макродефрмации более, чем в 2 раза меньше. На субструктурном уровне образование (TiMo)N твердого раствора также приводит к более высокой микродеформации в сравнении с аналогичным параметром в ZrN монометаллических слоях. Твердость многопериодных (TiMo)N/ZrN композитов достигает большой величина 35 ГПа.

1. Introduction

A feature of modern materials science of vacuum-plasma coatings is the use of multi-element [1, 2] and multi-layer [3, 4] approaches to create materials with desired properties. In this case, structural engineering of coatings is based both on a change in the composition and physicochemical conditions of formation [5, 6], and on a change in the thickness of the constituent elements, transfering it to the nanoscale [7, 8]. In a multi-layer design, to achieve enhanced properties, ultra-small (nanometer range) layer thicknesses are also used [9–11]. This allows achieving uniquely high functional properties, for example, ultrahigh hardness [12, 13].

For nanocomposites, an important role is played by the state of intergranular and interphase boundaries [14]. Especially important is the state of the layer interfaces in nanolayer multilayer composites [15, 16]. It was found that with similar crystal lattices with close periods (mismatch less than 3 %), quasiepitaxial layers can be formed up to sufficiently large thicknesses [17, 18]. Such composites have a sufficiently high ductility, however, their hardness is relatively not high [19, 20]. In this case, to change the period mismatch, it was proposed in [21] to alloy one of the layers. The main direction of such alloying was to reduce the mismatch between periods. For this, for example, a multi-period $V_{0.6}Nb_{0.4}N$/NbN composite was created in which, due to alloying, the mismatch was reduced from 5.7 % (for the VN/NbN composite without alloying) to 3.5 % for the alloyed composite [21]. However, this alloying led to a decrease in hardness.

Later in [22] it was shown that the strength and hardness of multi-period nanolayer coatings strongly depend on the width of the interface and the difference between the shear moduli of the two components.

Based on this, it was substantiated in [23] that the main mechanism of strengthening of nitride nanolayer coatings is determined by the limitation of dislocation motion either along the interface between layers and between layers, or inside a layer. Such a barrier to the movement of dislocations is the incoherent interface between the layers. With greater periods mismatch, it is possible to create conditions for the formation of an incoherent interface even for the thinnest layers.

For a multi-period TiN/ZrN system, a sufficiently large mismatch between the periods of the crystal lattices (about 8 %) leads to a loss of quasi-epitaxy at a layer thickness of more than 10 nm [24, 25].

In this work, for this type of composite, it is proposed to use alloying not to reduce the mismatch between layers, but to increase it. At the same time, an increase in the strength characteristics and hardness of such a composite can be expected. For this, it was proposed to alloy the TiN layer with Mo atoms (having a significantly smaller atomic radius of 0.139 nm compared with the atomic radius of titanium of 0.147 nm). As a result of a decrease in the lattice period in (TiMo)N layers, the mismatch at the layer interface can exceed 10 %, which leads to large deformation and can stimulate the creation of new structural states in the boundary region.

The aim of this work was to study the effect of layer thickness and the magnitude of the bias potential applied during its formation on the phase-structural state, micro-,

Table 1. Technological modes of deposition of coatings (TiMo)N/ZrN ($P_N = 4 \cdot 10^{-3}$ Torr)

Series No.	h, μm	l, nm	U_b, V	Operating mode of the substrate holder
1	12.4	12.7	−70	continuous rotation of substrates
2	12.1	12.4	−110	
3	11.8	12.1	−200	
4	12.8	21	−200	10 s interval 532 layers
5	13	380		160 s interval 34 layers

macrodeformation, and mechanical characteristics of the multi-period (TiMo)N/ZrN composite with a large degree of mismatch between the periods between layers.

2. Experimental

The coatings were deposited in the Bulat-6 vacuum-arc installation for 1.5 h at a working atmosphere pressure of $P_N = 4 \cdot 10^{-3}$ Torr. During the deposition, a different negative bias potential (U_b) was applied, which was −70 V, −110 V and −200 V. The multilayer coatings were deposited from two sources of evaporation, one of which was Zr, the other was TiMo (Mo — 30 wt.%) in constant rotation mode (rotation speed 8 rpm) and in discrete mode (with a stop near each source for 10 s and 160 s). The thickness of the layers (l) was determined by calculation based on the total thickness of the coating and the number of layers. The values obtained are shown in Table 1. Modes of obtaining coatings are given in Table 1, and the operation diagram of the installation during the deposition of (TiMo)N/ZrN composites is shown in Fig. 1. The total thickness of the coatings was about 12 microns.

The phase-structural state was investigated using X-ray diffractometry techniques. X-ray diffraction spectra were obtained on a DRON-4 setup in Cu–K_α radiation, using θ–2θ scanning in the range of angles 30...90°, with a scanning step of 0.1 deg and a holding time of 10 s. To monochromatize the detected radiation, we used a graphite monochromator installed in the secondary beam (in front of the detector) [26]. The separation of complex profiles into components was carried out using the NewProfile software package [27]. To determine the phase composition of the coatings, we used the data of powder diffraction files (JCPDS) published by the International Center for Diffraction Data (ICDD) [28]. Sub-

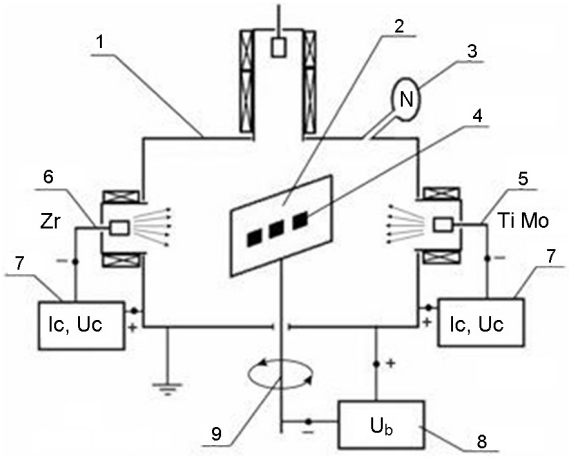

Fig. 1. The scheme of the installation during the deposition of (TiMo)N/ZrN multilayer composites: *1* — vacuum chamber, *2* — metal screen, *3* — nitrogen leak, *4* — deposited samples, *5* — TiMo evaporator, *6* — Zr evaporator, *7* — arc sources, *8* — a source of supply of potential to the substrate, *9* — rotary mechanism.

structural characteristics were determined by the approximation method [29].

To determine the elemental composition, the method of X-ray fluorescence analysis was used on the SPRUT-2 installation (Ukraine). The primary stimulating radiation was the radiation of an X-ray tube with an Ag anode at a voltage of 42 kV [30].

Hardness was measured on a DM-8 microhardness tester (Affri, Italy) using a Vickers diamond pyramid as an indenter at a load of 50 g, exposure time 10 s. For each sample, 10 measurements were performed.

3. Results and discussion

To determine the elemental composition of the coatings, the method of X-ray fluorescence spectroscopy was used [30]. The results of the analysis of elemental composition are shown in Table 2.

Table 2. The elemental composition of the coatings determined by X-ray fluorescence

Series No.	C, at %.			Ti/Mo	(Ti + Mo)/Zr
	Ti	Zr	Mo		
1	49,14	44,23	6,63	7,41	1,26
2	44.45	47.62	7.93	5.61	1.10
3	36.23	56.61	7.16	5.06	0.77
4	42,71	49,37	7,92	5.39	1,03
5	50.41	41.41	8.18	6.16	1.41

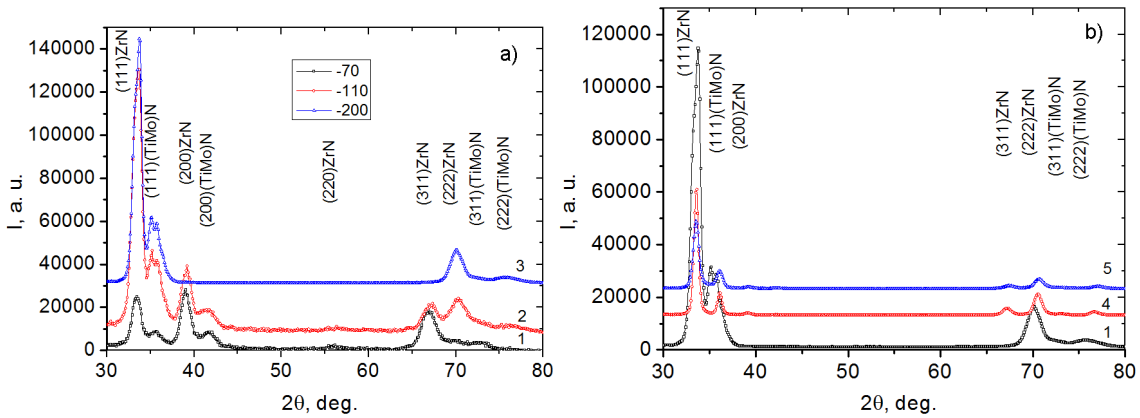

Fig. 2. XRD patterns of (TiMo)N/ZrN multi-period coatings obtained with different U_b (a) and layer thickness (b). The spectrum number in the figure corresponds to the sample number in Table 1.

As can be seen from the Table, the composition of coatings is significantly affected by both the value of U_b and the thickness of the coatings. If we assume that the ratio of atomic concentrations (Ti + Mo) and Zr corresponds to the average ratio of the thicknesses of the layers in the coating, then at $U_b = -200$ V the highest ratio (Ti + Mo)/Zr = 1.41 is associated with the thickest layers (TiMo)N in the coating of series 5. With a decrease in the layer thickness, this ratio sharply decreases. The second pattern that can be traced is a decrease in the ratio (Ti + Mo)/Zr with an increase in U_b. As a model explaining both of these dependences, the model of secondary selective atomization of atoms from the surface of layer formation can be used [16]. With selective sputtering in the energy range of 50–200 V, the greatest effect is associated with particles of greater mass. The atomic masses of Zr and Mo are almost 2 times the atomic mass of Ti. In this case, the heavier Zr atoms selectively sputter the lighter Ti atoms from the deposition surface. Moreover, the efficiency of such selective sputtering increases with increasing U_b and decreasing layer thickness. In the latter case, this is due to an increase in the number of such boundaries between the layers (Ti + Mo) and Zr with a decrease in the layer thickness. The reason for the observed effect can be associated with a change in the ratio between light Ti atoms and heavy Mo atoms as a result of selective sputtering from the growth surface with an increase in their average energy. As can be seen from Table 2, this effect is most noticeable in the thinnest layers with an increase in the bias potential from −70 V (series 1) to −200 V (series 3). An increase in the potential bias leads to an increase in the average energy of deposited particles and, accordingly, can change the sputtering efficiency for elements of different masses.

To study the phase-structural state of composite coatings, the X-ray diffraction method was used. Figure 2 (a and b) shows the areas of X-ray diffraction spectra of coatings with a similar layer thickness (about 13 nm) deposited at different U_b (Fig. 2a). The second figure (Fig. 2b) shows the X-ray diffraction spectra of the coatings deposited at $U_b = -200$ V, but with different layer thicknesses (Fig. 2b).

It can be seen that in the ZrN and (TiMo)N layers the same type fcc lattice forms (structural type B1–NaCl). A feature of the spectra for the thinnest layers (about 10 nm, continuous rotation mode) is the separation of diffraction peaks into several components. With increasing U_b, the separation effect increases. Also, with an increase in U_b, a texture is formed with the [111] axis both in ZrN layers and in (TiMo)N layers. With an increase in the thickness of the coating layers obtained at $U_b = -200$ V, the texture with the [111] axis is retained; however, peak separation is not detected.

For a more detailed study of the effect of separation into several components of diffraction profiles, processing was performed in the NewProfile software package [27] with the separation of components. Figure 3 shows the sections of the diffraction spectra after separation (decomposition) of the complex diffraction profile into components. To construct a model profile of the diffraction curve, the Cauchy function was used. It can be seen that for coatings with the smallest layer thickness (series 1, 2, and 3), the dif-

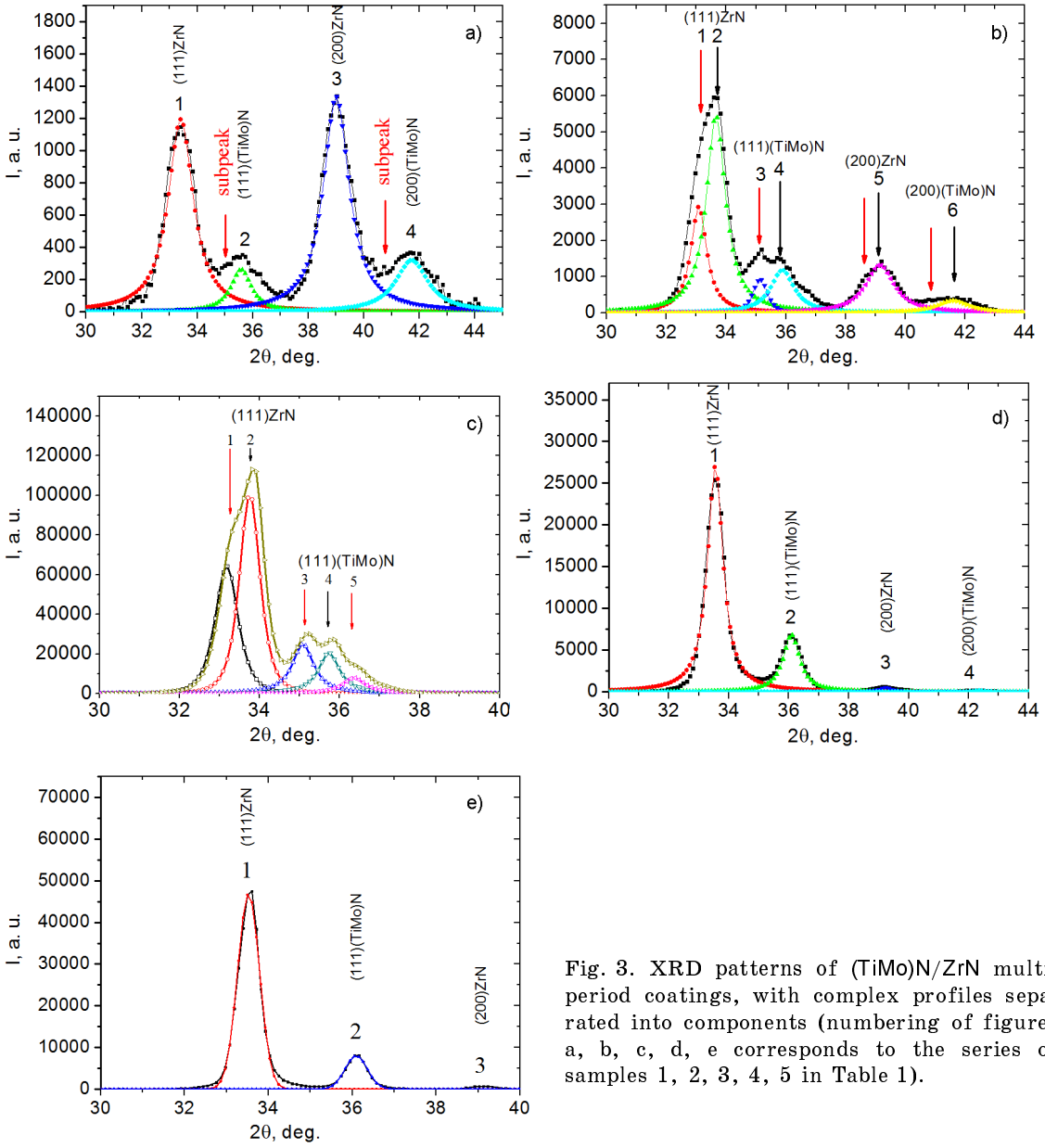

Fig. 3. XRD patterns of (TiMo)N/ZrN multi-period coatings, with complex profiles separated into components (numbering of figures a, b, c, d, e corresponds to the series of samples 1, 2, 3, 4, 5 in Table 1).

fraction profiles contain several distinct components. Moreover, with an increase in U_b, the intensity of these components increases and a greater number of them is revealed.

In the diffraction spectrum of the coating obtained at the lowest $U_b = -70$ V, the subpeak appears as a region with increased intensity (marked by an arrow in Fig. 3a).

The positions of the main peaks correspond to periods of 0.4615 nm (for the ZrN layer, peak numbers 1 and 3 in Fig. 3a) and 0.4323 nm (for the (TiMo)N layer, peak numbers 2 and 4 in Fig. 3a).

The texture with the [111] axis appears on the diffraction spectrum of the coating obtained at a larger $U_b = -110$ V (Fig. 3b), while the intensity of the sub-peaks increases. When dividing the total (111) ZrN profile, we obtain 2 components (Fig. 3b).

The first component (subpeak) with an increased period of 0.4679 nm, the volume content of which in the ZrN layer is about 23 % (determined by the ratio of the integral areas of the 1st and 2nd components). Note that one of the most probable reasons for the formation of such a component may be the formation of a alloyed layer with high compression stresses.

The position of the second peak corresponds to a grating period of 0.4607 nm, which correlates with the period for the (111) ZrN peak determined for the first series of coatings (Fig. 3a).

Table 3. The results of determining the substructural characteristics of coatings

Series No.	Phase	L, nm	<*epsilon*>, %
1	ZrN	13	0.62
	(TiMo)N	18	1.05
2	ZrN	15	0.65
	(TiMo)N	15	0.78
3	ZrN	11	0.52
	(TiMo)N	10	0.65
4	ZrN	23	0.51
	(TiMo)N	20	0.59

For the complex diffraction profile from the (111) (TiMo)N plane, two components are also clearly distinguished. The peak position for the 1st component corresponds to a lattice period of 0.442 nm (volume content of about 37 %), and the position of the second peak corresponds to a lattice period of 0.433 nm (volume content of about 63 %). The appearance of the first peak (subpeak) corresponding to the increased lattice period can also be the formation of a layer with high compression stresses. Similarly, the substitution of Ti atoms by Zr atoms having a larger atomic radius also affects.

For peaks from the (200) plane, due to their lower intensity, the effects of subpeaks are less pronounced (indicated by arrows in Fig. 3b).

The diffraction profiles from the [111] texture plane in the coating obtained at the highest $U_b = -200$ V are even more complex (Fig. 3c).

When the (111) ZrN profile is divided, 2 components are also revealed. Their peaks correspond to periods of 0.4678 nm and 0.4601 nm. However, their ratio (compared to coatings of series 2) is changed to 39/61. For the complex diffraction profile (111) (TiMo)N, 3 components are already detected. The first component (subpeak) corresponds to an increased period of 0.442 nm (which corresponds to the sub-peak period of the series 2 coating). The position of the second peak corresponds to a lattice period of 0.433 nm (which can be considered the main characteristic for all 3 series of coatings).

In contrast to the diffraction profile of the coating of the 2nd series, this profile is characterized by separation into the 3rd subpeak, the maximum position of which corresponds to the period of 0.4279 nm.

In the coating obtained with the same large bias potential, $U_b = -200$ V, but with a larger layer thickness (about 23 nm, series 4), no sub peaks are detected when diffraction profiles are selected (Fig. 3d). Possibly due to the fact that their contribution to the overall diffraction spectrum becomes lower.

The lattice period for ZrN, determined from the position of the (111) peak, is 0.4621 nm, and for (TiMo)N, it is 0.4310 nm.

For the coating with the thickest layers (series 5), the separation of the diffraction profiles into components is also not revealed (Fig. 3e), and a certain period of the lattice period practically coincides with the values for the series 4 coatings (for ZrN, the period is 0.4629 nm, and for (TiMo)N period is 0.43102 nm).

To determine the substructural characteristics (crystallite size and microdeformation), we used the method of approximating diffraction profiles for two orders of magnitude from the {111} planes. The results are shown in Table 3.

It can be seen that microdeformation in crystallites of the ZrN phase is about 0.5...0.65 %. In crystallites of the (TiMo)N phase, microdeformation is much larger (series 1, 2, and 3) and its value is almost 1.5 times larger than for ZrN. In the same coatings with the thinnest layers, the crystallite size was 11...15 nm, which corresponds to the average layer thickness. Also close to the thickness of the layer and the size of crystallites in the coatings of the 4th series (L = 21..23 nm). For the thickest layers (series 5 with an average layer thickness of about 360 nm), this ragularity is violated. The average crystallite size for series 5 coatings is close to similar parameters for series 4 coatings. For ZrN layers, the average crystallite size is 23 nm, and for (TiMo)N layers is 20 nm). An important characteristic that determines the properties of coatings is their stress-strain state. To determine it, we used the modernized "$a - \sin^2\psi$" method, which was developed for textured materials (the method of "crystalline groups" [31, 32]).

The results of determining the macrostrained state in ZrN and (TiMo)N layers are presented in Fig. 4. It can be seen that the multilayer composite coating is subjected to high compressive stresses, which leads to compression strain of the crystal lattice. To a lesser extent, this is manifested in ZrN layers and to a much greater extent in (TiMo)N layers. With an increase in the layer

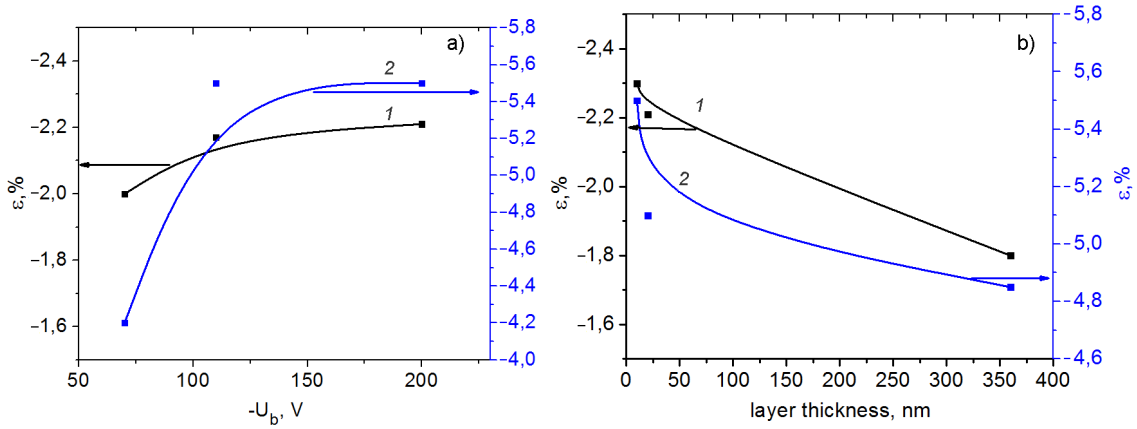

Fig. 4. Plots of macrostrain (ε) as a function of displacement potential (a) and layer thickness (b) of multilayer coatings. *1* — ZrN layer, *2* — (TiMo)N layer.

thickness, partial compression strain relaxation occurs (Fig. 4). A decrease in U_b also leads to a decrease in the stress-strain state.

The most universal characteristic of the physicomechanical properties of materials is their hardness. Determination of the hardness of the coatings showed that the highest value of 35 GPa is achieved in the coatings of the first series obtained with the smallest $U_b = -70$ V and the smallest layer thickness. With an increase in U_b to −200 V, the hardness of the coatings decreases slightly (up to 31 GPa). However, the hardness with the smallest layer thickness in series 3 is significantly higher than in coatings with a larger layer thickness (for the 4th series, the hardness of the coatings is 29 GPa, and for the 5th series the hardness is 25 GPa).

An analysis of the results shows that alloying of titanium nitride with molybdenum atoms to create large distortion of the crystal lattice manifests itself at both macro and micro levels. In this case, the macrostrain in the (TiMo)N layers is almost 2 times higher than the macrostrain in the ZrN layers, and for microstrain the excess is 1.5 times.

The effect of such a large strain and mismatch of the periods of the crystal lattices is most clearly manifested at the structural level for the thinnest (about 12 nm) layers obtained by continuous rotation of the substrate holder.

In this case, in the coatings deposited at all U_b values (−70 V, −110 V and −200 V), additional diffraction peaks are revealed with altered fixed lattice periods. This is manifested to the greatest extent in coatings deposited at the highest $U_b = -200$ V.

The reason for the appearance of such a separation can be the creation of a high level of deformation in the boundary region between the ZrN and (TiMo)N layers due to the implantation of atoms with very different atomic radii (this is mainly due to the replacement of Ti atoms by Zr and Mo atoms having a larger atomic radius).

4. Conclusions

By the method of vacuum-arc evaporation, multi-period (TiMo)N/ZrN coatings with different layer thicknesses and at different bias potentials U_b were obtained.

It was established that with an increase in U_b in the coatings, the relative content of heavier elements Zr and Mo increases. This effect is enhanced with decreasing layer thickness.

It was revealed that for all the technological conditions used in the work, in the (TiMo)N and ZrN layers, the formation of the same type of crystal structures based on the fcc metal lattice (structural type B1–NaCl) occurs.

The effect of separation into several components of diffraction profiles for coatings with layers with the smallest thickness is revealed. The established effect is associated with the process of surface implantation of accelerated film-forming metal particles and the formation of a strongly deformed state.

It was found that for coatings with relatively thick layers, the effect of separation of the diffraction profile into components is not detected.

At the substructural level, a significant increase in the microdeformed state was revealed in the (TiMo)N layers in comparison with the ZrN layers. It was found that for small layer thicknesses (up to 25 nm) the

crystallite size corresponds to the layer thickness. With a larger layer thickness, the average crystallite size is 35 nm (ZrN layer) and 43 nm ((TiMo)N layer).

It has been established that macrostrain in (TiMo)N layers is more than 2 times higher than the similar parameter in ZrN layers. With an increase in U_b, the magnitude of macrostrain increases.

It was determined that the highest hardness of 35 GPa is achieved in coatings with the lowest U_b and the smallest layer thickness. With an increase in U_b, as well as with an increase in the thickness of the layers, the hardness decreases.

References

1. C.Li, J.C.Li, M.Zhao, Q.Jiang, *J. Alloys Comp.*, **475**, 752 (2009).
2. J.W.Yeh, S.K.Chen, S.J.Lin et al., *Advan. Engin. Mater.*, **6**, 299 (2004).
3. O.V.Sobol', A.A.Andreev, V.F.Gorban, *Metal Sci. Heat Treat.*, **58**, 40 (2016).
4. O.V.Sobol', A.A.Andreev, V.F.Gorban et al., *J. Nano- Electron. Phys.*, **8**, 01042 (2016).
5. M.A.Glushchenko, E.V.Lutsenko, O.V.Sobol' et al., *J. Nano- Electron. Phys.*, **8**, 03015 (2016).
6. M.A.Glushchenko, V.V.Belozyorov, O.V.Sobol' et al., *J. Nano- Electron. Phys.*, **9**, 02015 (2017).
7. R.Kumar, Z.Ahmed, H.Kaur et al., *Catalys. Sci. Technol.*, **10**, 2213 (2020).
8. O.V.Sobol', O.Dur, *Functional Materials*, **27**, 100 (2020).
9. Y.Sun, Y.Chen, N.Tsuji, S.Guan, *J. Alloys Comp.*, **819**, 152956 (2020).
10. O.V.Sobol', A.A.Meylekhov, V.A.Stolbovoy, A.A.Postelnyk, *J. Nano- .Electron. Phys.*, **8**, 03039 (2016).
11. S.H.Wu, Z.Q.Hou, J.Y.Zhang et al., *Scripta Mater.*, **172**, 61 (2019).
12. J.Prochazka, P.Karvankova, G.M.Veprek-Heijman, S.Veprek, *Mater. Sci. Engin. A*, **384**, 102 (2004).
13. J.Xu, M.Kamiko, Y.Zhou et al., *J. Appl. Phys.*, **89**, 3674 (2001).
14. M.A.Zhadko, A.I.Zubkov, O.V.Sobol', *J. Nano- Electron. Phys.*, **10**, 03003 (2018).
15. P.H.Mayrhofer, C.Mitterer, J.G.Wen et al., *Appl. Phys. Lett.*, **86**, 131909-3 (2005).
16. O.Sobol', A.Meylekhov, A.Postelnyk, *Lecture Notes Mechan. Engin.*, 146 (2019).
17. O.V.Sobol', R.P.Mygushchenko, A.A.Postelnyk, *J. Nano- .Electron. Phys.*, **10**, 03009 (2018).
18. M.Shinn, L.Hultman, S.A.Barnett, *J. Mater. Res.*, **7**, 901 (1992).
19. Q.Yang, C.He, L.R.Zhao, J-P.Immarigeon, *Scripta Mater.*, **46**, 293 (2002).
20. Y.-Z.Tsai, J.-G.Duh, *Surf. Coat. Technol.*, **200**, 1683 (2005).
21. M.Shinn, S.A.Barnett, *Appl. Phys. Lett.*, **64**, 61 (1994).
22. Xi Chu, S.A.Barnett, *J. Appl. Phys.*, **77**, 4403 (1995).
23. W.D.Sproul, *Surf. Coat. Technol.*, **1**, 170 (1996).
24. O.V.Sobol', A.A.Meilekhov, *Techn. Phys. Lett.*, **44**, 63 (2018).
25. O.V.Sobol', A.A.Postelnyk, A.A.Meylekhov et al., *J. Nano- .Electron. Phys.*, **9**, 03003-1 (2017).
26. O.V.Sobol', O.A.Shovkoplyas, *Techn. Phys. Lett.*, **39**, 536 (2013).
27. M.V.Reshetnyak, O.V.Sobol', *PSE*, 6 (3-4) (2008).
28. http://www.icdd.com
29. I.C.Noyanand, J.B.Cohen, Springer-Verlag, NewYork (1987), p.350.
30. I.F.Mikhailov, A.A.Baturin, A.I.Mikhailov, S.S.Borisova, *Functional Materials*, **19**, 126 (2012).
31. C.Genzel, *Phys. Stat. Solidi (a)*, **159**, 283 (1997).
32. C.Genzel, W.Reinmers, *Phys. Stat. Solidi: A-Appl. Res.*, **166**, 751 (1998).